Population inversion in N_2^+ by vibrationally mediated Rabi oscillation at 400 nm

Siqi Wang,[1,*] Erik Lötstedt,[2,*] Jincheng Cao,[1] Yao Fu,[1] Hongwei Zang,[1] Helong Li,[1,3] Toshiaki Ando,[2] Atsushi Iwasaki,[2] Kaoru Yamanouchi,[2,†] and Huailiang Xu[1,4,5,‡]

[1]*State Key Laboratory of Integrated Optoelectronics, College of Electronic Science and Engineering, Jilin University, Changchun 130012, China*

[2]*Department of Chemistry, School of Science, The University of Tokyo, 7-3-1 Hongo, Bunkyo-ku, Tokyo 113-0033, Japan*

[3]*Institute of Atomic and Molecular Physics, Jilin University, Changchun 130012, China*

[4]*State Key Laboratory of Precision Spectroscopy & Chongqing Institute, East China Normal University, Shanghai 200062, China*

[5]*CAS Center for Excellence in Ultra-Intense Laser Science, Shanghai 201800, China*

(Received 4 July 2021; accepted 24 August 2021; published 24 September 2021)

We investigate lasing of a nitrogen gas induced by intense femtosecond laser pulses at around 400 nm. By examining both the self-induced and externally seeded forward emission spectra, we unambiguously identify the N_2^+ lasing actions at 427.8 and 423.6 nm assigned respectively to the $B\,^2\Sigma_u^+ - X\,^2\Sigma_g^+$ (0, 1) and (1, 2) emissions and show that the lasing mechanism is totally different from the lasing induced by near-infrared (800 nm) laser pulses, in which the population transfer from $X\,^2\Sigma_g^+$ to $A\,^2\Pi_u$ proceeds through the resonant $X\,^2\Sigma_g^+ - A\,^2\Pi_u$ transition, facilitating the population inversion between the $B\,^2\Sigma_u^+ - X\,^2\Sigma_g^+$ states [Phys. Rev. Lett. **123**, 203201 (2019)]. We simulate the population distributions among the vibrational levels in the three lowest electronic states of N_2^+ by the 400-nm laser pumping and find that the population is efficiently transferred between the $X\,^2\Sigma_g^+$ state and the $B\,^2\Sigma_u^+$ state by a Rabi oscillation combined with a Raman-type transition, leading to the population inversion so that the lasing occurs at the $B\,^2\Sigma_u^+ - X\,^2\Sigma_g^+$ (0, 1) and (1, 2) emissions.

DOI: 10.1103/PhysRevA.104.032823

I. INTRODUCTION

Optical amplification produced during the nonlinear propagation of ultrashort laser pulses in air is promising in identifying and quantifying atmospheric pollutants for environmental monitoring [1–5]. It was demonstrated that in ultrashort intense laser fields the two major atmospheric constitutes, i.e., N_2 and O_2, can be excited, ionized, and dissociated, producing population-inverted O and N atoms, N_2 molecules and N_2^+ molecular ions, and inducing lasing emissions in air called "air lasing" [2,3,5–12]. In particular, the lasing actions in N_2^+ have gained special interests because of the complex mechanism by which the lasing action is realized.

So far, a variety of different mechanisms have been proposed such as population inversion [13–18], rotational coherence [19,20], and lasing without inversion [21,22]. When it comes to the lasing at 391 nm of N_2^+, recent publications revealed that the first electronically excited $A\,^2\Pi_u$ state of N_2^+ plays a crucial role in creating the inverted population between the $B\,^2\Sigma_u^+$ and $X\,^2\Sigma_g^+$ states in an near-IR (800 nm) ultrashort laser field, leading to the $B\,^2\Sigma_u^+ - X\,^2\Sigma_g^+$ (0, 0) lasing emission at 391 nm [14,16,21,23–31] through the resonant population transfer from the $X\,^2\Sigma_g^+$ state to the $A\,^2\Pi_u$ state via the $X\,^2\Sigma_g^+ - A\,^2\Pi_u$ transition [23]. Indeed, by modulating the population transfer process from the $X\,^2\Sigma_g^+$ state to the $A\,^2\Pi_u$ state, we showed that the lasing intensity at 391 nm, corresponding to the $B\,^2\Sigma_u^+$ ($\upsilon' = 0$)-$X\,^2\Sigma_g^+$ ($\upsilon'' = 0$) transition, can be enhanced by a few orders of magnitude or more [23,25,30]. It is now commonly understood that the N_2^+ lasing in a near-IR ultrashort intense laser field is realized by the coherent coupling of the three electronic states via the $B\,^2\Sigma_u^+ - X\,^2\Sigma_g^+ - A\,^2\Pi_u$ scheme [23].

On the other hand, it was reported that the N_2^+ lasing at 391 nm can also be generated in air by the irradiation with intense laser pulses at wavelengths of 400 nm [32], 1 μm [20], and 3.9 μm [20], by which the resonant optical coupling between the $X\,^2\Sigma_g^+$ and $A\,^2\Pi_u$ states cannot be achieved. In the cases of 1 μm and 3.9 μm [20], it was proposed that the transient inversion between the rotation levels of the electronically exited $B\,^2\Sigma_u^+$ state and those in the $X\,^2\Sigma_g^+$ state of N_2 plays a key role in the lasing at 391 nm. However, no detailed explanation of the mechanism of the lasing at 391 nm induced by the irradiation of intense 400-nm laser pulses has been made so far. Because the photon energy at 400 nm is twice as large as the energy gap between the $X\,^2\Sigma_g^+$ and $A\,^2\Pi_u$ states and is almost equal to the energy gap between the $X\,^2\Sigma_g^+$ and $B\,^2\Sigma_u^+$ states, it is worthy to examine how the population inversion between the $B\,^2\Sigma_u^+$ and $X\,^2\Sigma_g^+$ states can be achieved without the participation of the $A\,^2\Pi_u$ state.

In the present study, by irradiating a N_2 gas with an intense near-UV field at around 400 nm, we observe two lasing lines of N_2^+ at 423.6 and 427.8 nm, corresponding,

*These authors contributed equally to this work.
†kaoru@chem.s.u-tokyo.ac.jp
‡huailiang@jlu.edu.cn

respectively, to the $B\,^2\Sigma_u{}^+(\upsilon'=1)$–$X\,^2\Sigma_g{}^+(\upsilon''=2)$ and $B\,^2\Sigma_u{}^+(\upsilon'=0)$–$X\,^2\Sigma_g{}^+(\upsilon''=1)$ emissions. We further examine the two lasing lines by shooting a seed beam in a cross angle of 4° with respect to the pumping beam in a noncollinear scheme to achieve the externally seeded lasing actions at the two lasing lines. By solving the time-dependent Schrödinger equation, we simulate the population distributions of the vibrational levels in the $B\,^2\Sigma_u{}^+$, $A\,^2\Pi_u$, $X\,^2\Sigma_g{}^+$ states of $N_2{}^+$ and reveal that the population inversion in $N_2{}^+$ can be achieved by the light-induced $B\,^2\Sigma_u{}^+$–$X\,^2\Sigma_g{}^+$ coupling after the ionization of neutral N_2 by the resonance Rabi oscillation mediated by Raman-type vibrational pumping. This is a mechanism characteristic to molecular systems in which the vibrational motion is coupled with the Rabi oscillation between two electronic states. Our experimental and theoretical study confirms that the population inversion between the $B\,^2\Sigma_u{}^+$ state and the $X\,^2\Sigma_g{}^+$ state in $N_2{}^+$ can be created by an ultrashort intense 400-nm laser pulse even in the absence of the population depletion in the $X\,^2\Sigma_g{}^+$ state by the optical pumping to the $A\,^2\Pi_u$ state through the $A\,^2\Pi_u$–$X\,^2\Sigma_g{}^+$ transition.

II. EXPERIMENT

A. Experimental setup

The experiments were performed by using a Ti:sapphire laser system (Spectra Physics, Spitfire ACE), which produced femtosecond laser pulses at a repetition rate of 200 Hz, a central wavelength of 800 nm, a pulse energy of up to 8 mJ, a pulse duration of ~40 fs, and a beam diameter of 7 mm. The laser beam was split into two arms by a 9:1 beam splitter. The higher-energy beam first passed through a beta-barium-borate (β-BBO) crystal (thickness 200 μm; diameter 10 mm) to be frequency doubled, producing laser pulses at around 395 nm, which is hereafter called 400-nm pulses. The resultant pulse was separated from the fundamental 800-nm laser by a dichroic mirror with high reflectivity at around 400 nm and high transmission at around 800 nm. The energy of the 400-nm pulses was controlled by adjusting the fundamental laser energy using a half-wave plate and a polarizer. The maximum energy of the 400-nm pulses was 1.3 mJ, which were adopted as the pump pulses, generating the population inversion in $N_2{}^+$.

The pump beam was focused by a fused silica lens of $f = 30$ cm into a chamber filled with a pure N_2 gas at 200 mbar, as shown in Fig. 1(a). In the pump-probe measurements, the weaker energy beam was also frequency doubled in another β-BBO crystal to generate the seed pulse at around 400 nm with an energy of ~2 μJ. We adopted a noncolinear scheme with the external seeding to avoid possible nonlinear interaction processes of the two laser pulses. The seed pulse was focused by another fused silica lens of $f = 30$ cm and crossed the pump pulse at an angle of 4°, as shown in Fig. 1(b). The temporal delay between the pump and seed pulses was finely controlled by a motorized delay line installed in the seed arm with a temporal resolution of about 10 fs. The polarization direction of the seed pulse was tuned to be parallel with that of the pump pulse by a half-wave plate for 400 nm.

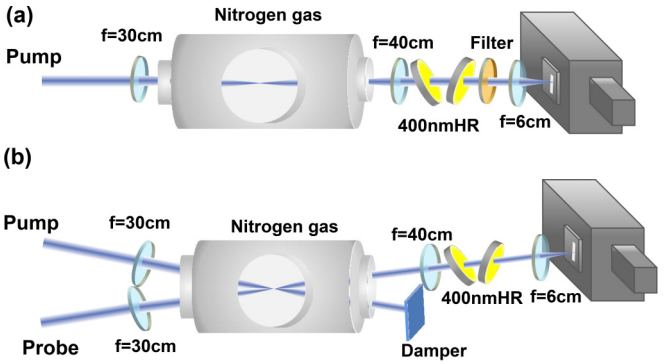

FIG. 1. Schematics of the experimental setups for (a) self-seeding and (b) external-seeding lasing actions with the pumping by 400-nm ultrashort laser pulses.

The forward light generated either along the pump beam in the self-seeding scheme [see Fig. 1(a)] or along the probe beam in the pump-seed scheme [see Fig. 1(b)] was collimated using a fused silica lens of $f = 40$ cm. Two mirrors with high reflectivity at around 400 nm were used to reflect the pump/probe pulse(s) while transmitting the generated lasing signal at 422–428 nm. For the self-seeding scheme shown in Fig. 1(a), the light was further attenuated using a neutral density filter. In both schemes shown in Figs. 1(a) and 1(b), the lasing light was focused by a fused silica lens of $f = 6$ cm onto the entrance slit of a spectrometer (Andor Shamrock SR-303i) equipped with a 1200-grooves/mm grating, and the dispersed spectrum was recorded by an ICCD camera (Andor iStar). The slit width of the spectrometer was set at 150 μm, and the ICCD gate delay was opened at $t = -10$ ns before the laser pulse arrives at the interaction zone, and the ICCD gate width was set at $\Delta t = 50$ ns to eliminate the signals originating from the scattering light. For all the measurements, the data were accumulated over 400 laser shots.

B. Experimental results

In Fig. 2(a) we show the forward emission spectrum in the wavelength range of 421–430 nm obtained by the scheme in Fig. 1(a). In the measurement, the laser energy was set at 0.6 mJ and the laser spectrum was centered at 394.5 nm with the bandwidth of ~4.5 nm at full-width at half-maximum as shown in the inset of Fig. 2(a). The pulse duration was estimated to be about 50 fs from the measured laser bandwidth, assuming that the pulse had a transform-limited Gaussian distribution. The shortest pulse duration was determined by the analysis of the pump-laser-induced fluorescence intensity of $N_2{}^+$ [33]. It can be seen in Fig. 2(a) that two lasing lines at around 423.6 and 427.8 nm appear, which can be assigned respectively to the $B\,^2\Sigma_u{}^+$–$X\,^2\Sigma_g{}^+$ (1, 2) and (0, 1) emission transitions, as explained in Fig. 2(b). The $B\,^2\Sigma_u{}^+$–$X\,^2\Sigma_g{}^+$ (0, 0) lasing emission expected to appear at 391 nm cannot be identified in the present experiment because of the spectral overlap with the pump laser pulses. We examined the lasing actions at different laser energies from 0.6 to 1.3 mJ. As shown in Fig. 2(c), both of the signal intensities at 423.6 and 427.8 nm increase as the laser energy increases. We also plot the intensities of the two lasing lines as a function of the

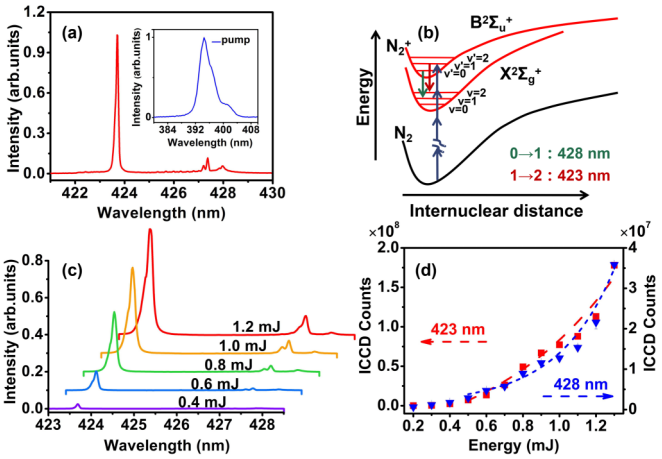

FIG. 2. (a) Self-seeded lasing spectrum of N_2^+ induced by a 394.5-nm pump laser field. Inset: the pump laser spectrum. (b) Energy-level diagrams of N_2^+ and N_2, and the corresponding lasing transitions. (c) Lasing spectra of N_2^+ measured at the different laser energies. (d) Integrated 423-nm (red square) and 428-nm (blue triangle) intensities as a function of the pump laser energy, which are respectively fitted to an exponential function.

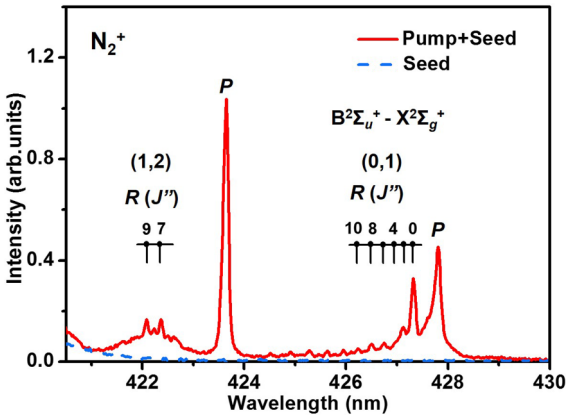

FIG. 3. The rotationally resolved lasing lines assigned to the $B^2\Sigma_u^+ - X^2\Sigma_g^+$ (1, 2) and (0, 1) transitions at around 423.6 and 427.8 nm in the forward spectra recorded in the seed arm with (red solid line) and without (blue dashed line) the 400-nm pump laser field. The rotational assignments of the R-branches are shown, in which J'' stands for the rotational quantum number in the $X^2\Sigma_g^+$ state.

pump laser energy as shown in Fig. 2(d). The signal intensities were accumulated over the spectral ranges of 421.9–424.3 nm and 424.7–428.7 nm, covering the respective rotational structures of the lasing lines at 423.6 and 427.8 nm. It can be seen in Fig. 2(d) that these two plots are well fitted to an exponential function. The results shown in Figs. 2(a), 2(c), and 2(d) indicate that the population inversion in N_2^+ can be achieved by the 400-nm laser field even in the absence of the $X^2\Sigma_g^+ - A^2\Pi_u$ coupling. It should be noted that the lasing action at 423.6 nm, induced by the 400-nm excitation, is not realized by the 800-nm excitation, and that the intensity of the lasing at 423.6 nm is stronger than that at 427.8 nm.

As one of the mechanisms of the air lasing, the lasing without population inversion was proposed [21]. In order that the lasing without population inversion between the $B^2\Sigma_u^+$ and $X^2\Sigma_g^+$ states is achieved, the V-shaped $B^2\Sigma_u^+ - X^2\Sigma_g^+ - A^2\Pi_u$ coupling of the three electronic states of N_2^+ is required. However, the V-shaped coupling cannot be realized at 400 nm because the $A^2\Pi_u$ and $X^2\Sigma_g^+$ states cannot be coupled optically. Therefore we can exclude the mechanism of the lasing without population inversion in the present case. Another possible mechanism of the population inversion is that called rotational quantum beat lasing without inversion [22]. However, considering that the rotational quantum beat lasing can only be achieved at around the half and quarter revivals of the molecular alignment and that the pump-seed delay of 420 fs in the present case does not match the quarter revival of N_2^+ at ~2 ps [24], we can also exclude this possibility.

In the self-seeding amplification scheme, the lasing intensity I_{laser} can be described by $I_{\text{laser}} = I_{\text{seed}}\exp(gL)$, where g is the optical gain coefficient of the medium and L is the length of the gain medium. As the input laser energy increases, the plasma length, i.e., the gain medium length L, increases, which induces an increase in the energy of the white light generated by the self-phase modulation effect, resulting in a higher-intensity self-seed pulse, I_{seed} [34]. The gain coefficient $g = \sigma \times \Delta n$, where σ is the cross section of the stimulated emission and Δn is the population difference between the upper and lower states, can be regarded as a constant because σ is a constant for a given type of transition and Δn is also a constant under the current experimental conditions due to the intensity clamping of the laser field [35]. Therefore the exponential increase in the intensities of the 423- and 428-nm lasing shown in Fig. 2(d) can be ascribed to the increase in L.

In the self-seeded scheme or a collinear pump-seed scheme, it is difficult to exclude other nonlinear effects such as stimulated Raman scattering [13] and lasing without population inversion [21]. Therefore we carried out a pump-seed measurement in a noncollinear scheme [see Fig. 1(b)] to verify the population inversion mechanism of N_2^+ in the intense 400-nm laser pumping. Figure 3 shows the forward spectra of the seed arm in the presence (solid red line) and absence (dashed blue line) of the pump laser pulses. In the measurement, the energies of the pump and seed laser pulses were set at 1 mJ and 2 μJ, respectively. The very weak seed pulse can guarantee that it cannot induce ionization of neutral N_2 molecules and its spectrum extends to about 430 nm. Therefore this weak pulse can serve as the seed to be amplified. The polarization directions of the pump and seed pulses were set to be parallel with each other. The pump pulse was introduced about 420 fs prior to the probe pulse to avoid the interference effect between the pump and seed pulses and the effect of molecular alignment on the N_2^+ lasing induced by the pump pulses, because at the delay of 420 fs, which is sufficiently earlier than the quarter revival time of ~2 ps [24], the N_2^+ ensemble exhibits an isotropic alignment distribution of $\langle\cos^2\theta\rangle \sim 0.33$, that is, the N_2^+ ensemble is neither aligned nor antialigned.

It can be seen in Fig. 3 that when the pump pulse is turned on, rotationally resolved lasing emissions assigned to the $B^2\Sigma_u^+ - X^2\Sigma_g^+$ (1, 2) and (0, 1) transitions appear at around 423.6 and 427.8 nm, which can be regarded as clear evidence of the building-up of the population inversion in

N_2^+ in the intense 400-nm field. The sharp peaks appearing at 423.6 and 427.8 nm are assigned to the P-branch heads of the rotational structure of the respective electronic transitions, in which the rotational transitions with $\Delta J = J'–J'' = -1$ appear close to each other, and the weaker and broader structures appearing at around 423.6 and 427.8 nm in the higher-energy side of the respective P-branch transitions are assigned to the rotational structure of the R-branch transitions with $\Delta J = J'–J'' = 1$. The assignment of the rotational quantum numbers, J'', are shown in Fig. 3. The rotational assignment of the R-branch transitions were made based on the simulation of the rotational structures using the spectroscopic constants of N_2^+: $B_e'' = 1.9318\,\mathrm{cm}^{-1}$, $\alpha_e'' = 0.0190\,\mathrm{cm}^{-1}$, $B_e' = 2.0845\,\mathrm{cm}^{-1}$, and $\alpha_e' = 0.0213\,\mathrm{cm}^{-1}$ [36].

In order to interpret the population inversion mechanism and provide the information necessary for numerical simulations, we estimate the laser intensity in the experiment. First, we estimate the energy threshold for the self-focusing effect of the 400-nm laser pulses when the filamentation occurs. The critical power P_{cr} for the self-focusing of the laser pulse is related to λ^2/n_2, where λ is the input laser wavelength and n_2 the Kerr nonlinear index [37]. The critical power P_{cr} for a 42-fs and 800-nm laser pulse in air was measured to be 10 GW [37], and under the focusing condition of our experiment where the f number is about 43, the clamping intensity at 800 nm was estimated to be 200–400 $\mathrm{TW/cm^2}$ [38]. The Kerr nonlinear index n_2 for a 400-nm laser pulse in air is about 1.3 times larger than that for an 800-nm laser pulse [33]. By scaling the above results, the critical power P_{cr} for the self-focusing in a N_2 gas at 200 mbar achieved by a 50-fs and 400-nm laser pulse is estimated to be $(400/800)^2/(1.3 \times 200/1000) \times 10\,\mathrm{GW} = 9.6\,\mathrm{GW}$, and consequently, we obtain the energy threshold for the self-focusing of the laser pulse at around 400 nm to be about 0.5 mJ. We have confirmed experimentally that the energy threshold of the self-focusing is about 0.5 mJ by observing the shift of the focal position of the pumping laser pulses towards the direction opposite to the laser propagation direction in a similar manner as that adopted in [39]. This means that, in the pulse energy range of 0.6–1.3 mJ in our experiment, filamentation occurs and that the laser intensity inside the filament core is clamped at a constant value. Because the clamping intensity of the filament generated at 800 nm was about 2.5 times higher than that of the filament generated at 400 nm [33], the clamping intensity in our experiment is estimated to be about 80–160 $\mathrm{TW/cm^2}$.

III. THEORY

A. Theoretical model

In order to interpret theoretically the experimental finding that population inversion can be simultaneously achieved for the $B\,^2\Sigma_u^+$–$X\,^2\Sigma_g^+$ (1, 2) and (0, 1) lasing emissions, we conduct numerical simulations based on the postionization three-state coupling model introduced in [14]. We solve the time-dependent Schrödinger equation for the amplitudes $c_{\alpha v}(t)$ of the vibronic states of N_2^+,

$$i\hbar\frac{dc_{\alpha v}(t)}{dt} = E_{\alpha v}c_{\alpha v}(t) - F(t)\sum_{\alpha'=X,A,B}\sum_{v'=0}^{v_{\max}}\mu_{\alpha v\alpha' v'}c_{\alpha' v'}(t), \tag{1}$$

where α (= X, A, or B) labels the electronic state, v the vibrational state, $E_{\alpha v}$ denotes the energy of the vibronic state $\alpha(v)$, and $\mu_{\alpha v\alpha' v'}$ is the transition dipole moment between the states $\alpha(v)$ and $\alpha'(v')$. The numerical values of $E_{\alpha v}$ are obtained from the experimentally determined Morse parameters of the potential energy curves of the $X\,^2\Sigma_g^+$, $A\,^2\Pi_u$, and $B\,^2\Sigma_u^+$ states [40], and the numerical values of $\mu_{\alpha v\alpha' v'}$ were calculated based on the data in [41,42]. We include vibrational states up to $v_{\max} = 4$ in each of the three potential energy curves and assume that the direction of the molecular axis is fixed at an angle θ with respect to the polarization direction of the laser field. The amplitude of the laser electric field $F(t)$ is defined as $F(t) = F_0 e^{-t^2/\tau^2}\cos(\omega t)$. We adopt the experimental parameters $\omega = 4.77\,\mathrm{rad/fs}$ corresponding to a wavelength of 394.5 nm and $\tau = 42.5$ fs corresponding to an intensity FWHM of $\tau_{\mathrm{FWHM}} = 50$ fs. The simulation is started at $t = 0$, assuming prompt ionization $N_2^+(X\,^2\Sigma_g^+) \leftarrow N_2(X\,^1\Sigma_g^+)$ at the peak of the pulse, and the time propagation is continued until $t_{\mathrm{final}} = 150$ fs. The initial values of the amplitudes $c_{X0}(t=0) = 0.972$, $c_{X1}(t=0) = 0.229$, $c_{X2}(t=0) = 0.0441$, $c_{X3}(t=0) = 0.0081$, and $c_{X4}(t=0) = 0.0016$ in the $X\,^2\Sigma_g^+$ state are given by the square roots of the Franck-Condon factors of the ionization process, and $c_{\mathrm{A}v}(t=0) = c_{\mathrm{B}v}(t=0) = 0$. It has been known that electronically excited states can be populated by the strong-field ionization [43]. In order to examine the contribution of the strong-field ionization to the formation of the electronically excited states of N_2^+, we have estimated the rate $\Gamma(\alpha)$ of the multiphoton ionization process, $N_2^+(\alpha) \leftarrow N_2(X\,^1\Sigma_g^+)$, by the length gauge MO-SFA formula [44]. At $\theta = 0^\circ$, we obtain the relative ionization probabilities of $\Gamma(X\,^2\Sigma_g^+) = 95.3\%$, $\Gamma(A\,^2\Pi_u) = 0.9\%$, and $\Gamma(B\,^2\Sigma_g^+) = 3.8\%$, where the rates are normalized according to $\Gamma(X\,^2\Sigma_g^+) + \Gamma(A\,^2\Pi_u) + \Gamma(B\,^2\Sigma_g^+) = 1$, which clearly shows that N_2^+ is dominantly created in the electronic ground $X\,^2\Sigma_g^+$ state and that the contribution of the strong-field ionization to the formation of the inverted population between the $B\,^2\Sigma_u^+$ and $X\,^2\Sigma_g^+$ states of N_2^+ is negligibly small.

B. Time-dependent populations

In Fig. 4 we show the time-dependent populations $p_{\alpha v}(t) = |c_{\alpha v}(t)|^2$ obtained when the peak laser field intensity is $I = 8 \times 10^{13}\,\mathrm{W/cm^2}$ and the alignment angles are $\theta = 0^\circ$ and $\theta = 65^\circ$. The initial populations are $p_{X0}(t=0) = 94.6\%$, $p_{X1}(t=0) = 5.2\%$, and $p_{B0}(t=0) = p_{B1}(t=0) = 0$. In Fig. 4(a) we can see that the population dynamics can be understood as a simultaneous Rabi oscillation in the resonant $B\,^2\Sigma_u^+(0)$–$X\,^2\Sigma_g^+(0)$ and $B\,^2\Sigma_u^+(1)$–$X\,^2\Sigma_g^+(1)$ transitions. The energy differences are $E_{\mathrm{B0}} - E_{X0} = 3.17$ eV and $E_{B1} - E_{X1} = 3.19$ eV, both of which are very close to the laser photon energy of $\hbar\omega = 3.14$ eV. The Rabi frequencies are calculated to be $\Omega_{B0X0} = F_0\mu_{B0X0}/2\hbar = 0.59$ rad/fs and $\Omega_{B1X1} = F_0\mu_{B1X1}/2\hbar = 0.35$ rad/fs, corresponding to the Rabi periods of $T_{B0X0} = 2\pi/\Omega_{B0X0} = 10.6$ fs and $T_{B1X1} = 2\pi/\Omega_{B1X1} = 18.0$ fs. Because of the presence of the off-resonant $B\,^2\Sigma_u^+(0)$–$X\,^2\Sigma_g^+(1)$ and $B\,^2\Sigma_u^+(1)$–$X\,^2\Sigma_g^+(0)$ couplings, the population can also be transferred from $X\,^2\Sigma_g^+(0)$ to $X\,^2\Sigma_g^+(1)$ by a Raman-type $X\,^2\Sigma_g^+(0)$–$B\,^2\Sigma_u^+(0\text{ or }1)$–$X\,^2\Sigma_g^+(1)$ transition.

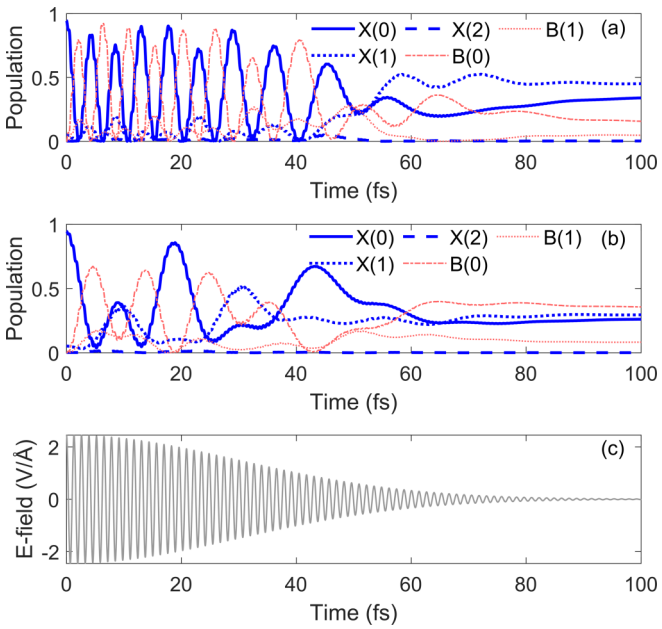

FIG. 4. Time-dependent populations in the $X\,^2\Sigma_g^+$ ($v = 0, 1, 2$) and $B\,^2\Sigma_u^+$ ($v = 0, 1$) states for the alignment angles at (a) $\theta = 0°$ and (b) $\theta = 65°$. (c) The laser electric field adopted in the simulation. The peak laser intensity is $I = 8 \times 10^{13}$ W/cm^2.

By the combination of this Raman-type $X\,^2\Sigma_g^+(0)$-$B\,^2\Sigma_u^+(0$ or 1)-$X\,^2\Sigma_g^+(1)$ transition and the resonant Rabi oscillation $X\,^2\Sigma_g^+(1)$–$B\,^2\Sigma_u^+(1)$, the population can be transferred from the $X\,^2\Sigma_g^+(0)$ state to the $B\,^2\Sigma_u^+(1)$ state. As shown in Fig. 4(a), the final population in the $B\,^2\Sigma_u^+(1)$ state is $p_{B1}(t_{\rm final}) = 4.6\%$. The population of the $X\,^2\Sigma_g^+(2)$ state is smaller than 5% when $t < 150$ fs, and the final population is calculated to be $p_{X2}(t_{\rm final}) = 0.27\%$. The reason for the small value of p_{X2} is that the $B\,^2\Sigma_u^+(0)$–$X\,^2\Sigma_g^+(2)$ transition is off resonance ($E_{B0} - E_{X2} = 2.63$ eV) and that its Franck-Condon factor is small. Indeed, the Franck-Condon factor, $|\langle B(0)|X(2)\rangle|^2 = 0.068$, is much smaller than $|\langle B(0)|X(1)\rangle|^2 = 0.26$ for the $B\,^2\Sigma_u^+(0)$–$X\,^2\Sigma_g^+(1)$ transition and $|\langle B(0)|X(0)\rangle|^2 = 0.66$ for the $B\,^2\Sigma_u^+(0)$–$X\,^2\Sigma_g^+(0)$ transition. As a result of the small population in the $X\,^2\Sigma_g^+(2)$ state and the population transfer to the $B\,^2\Sigma_u^+(1)$ state by the combination of the Rabi oscillation and the Raman-type transition, a final population inversion of $\Delta p_{B1X2} = p_{B1}(t_{\rm final}) - p_{X2}(t_{\rm final}) = 4.3\%$ is achieved, which explains the experimentally recorded lasing at 423.6 nm.

In Fig. 4(b) we show the time-dependent populations when $\theta = 65°$. Because the molecular axis is not aligned along the laser field polarization direction, the Rabi frequencies of the parallel $B\,^2\Sigma_u^+$–$X\,^2\Sigma_g^+$ transitions become smaller by a factor of $\cos 65° = 0.42$, so that the Rabi periods become $T_{B0X0} = 25.0$ fs and $T_{B1X1} = 42.6$ fs. As can be seen in Fig. 4(b), this longer Rabi period leads to a population inversion both between the $B\,^2\Sigma_u^+(0)$ and $X\,^2\Sigma_g^+(1)$ states and between the $B\,^2\Sigma_u^+(1)$ and $X\,^2\Sigma_g^+(2)$ states, and consequently, the final population differences become $\Delta p_{B0X1} = 5.6\%$ and $\Delta p_{B1X2} = 8.3\%$. This means that population inversion can occur simultaneously between the $B\,^2\Sigma_u^+(0)$ and $X\,^2\Sigma_g^+(1)$ states and between the $B\,^2\Sigma_u^+(1)$ and $X\,^2\Sigma_g^+(2)$ states.

In both cases ($\theta = 0°$ and $\theta = 65°$) shown in Fig. 4, the population in the $A\,^2\Pi_u$ state is negligibly small. In Fig. 4(a), $p_{Av}(t) = 0$ for all the five vibrational levels in the $A\,^2\Pi_u$ state, because the molecular axis is parallel to the polarization direction of the laser field, reflecting the fact that the transition dipole moment of the $A\,^2\Pi_u$–$X\,^2\Sigma_g^+$ transition is perpendicular to the molecular axis. In Fig. 4(b), the total population in the $A\,^2\Pi_u$ state is smaller than 3% in the entire range of t, and the final total population summed over all the vibrational states is $\sum_{v=0}^{v_{\rm max}} p_{Av}(100\ {\rm fs}) = 0.33\%$. In this case of $\theta = 65°$, the small $A\,^2\Pi_u$ state population is ascribed to the fact that the laser photon energy $\hbar\omega = 3.14$ eV is much larger than the energy gap between the $A\,^2\Pi_u$ state and the $X\,^2\Sigma_g^+$ state (for example, $E_{A0} - E_{X0} = 1.12$ eV), and consequently, the $A\,^2\Pi_u$–$X\,^2\Sigma_g^+$ transition cannot proceed efficiently.

C. Conditions for population inversion

In order to investigate further the conditions with which the population inversion between the $B\,^2\Sigma_u^+(0)$ state and the $X\,^2\Sigma_g^+(1)$ state and that between the $B\,^2\Sigma_u^+(1)$ state and the $X\,^2\Sigma_g^+(2)$ state are achieved, we calculate the final populations in the $X\,^2\Sigma_g^+(v'' = 0, 1, 2)$ and $B\,^2\Sigma_u^+$ ($v' = 0, 1$) states at different sets of the laser parameters.

The final populations in the vibrational levels in the $X\,^2\Sigma_g^+$, $B\,^2\Sigma_u^+$ and $A\,^2\Pi_u$ states depend on the laser intensity I, the alignment angle θ, and the pulse width $\tau_{\rm FWHM}$. However, because the $A\,^2\Pi_u$ state has a negligible effect on the population transfer dynamics, a change in the alignment angle θ is equivalent to a change in the $B\,^2\Sigma_u^+$–$X\,^2\Sigma_g^+$ coupling strength by a factor of $\cos\theta$. This means that the final population difference $\Delta p_{BvXv'}(I, \theta, \tau_{\rm FWHM})$ between the $B\,^2\Sigma_u^+$ and $X\,^2\Sigma_g^+$ states calculated at an intensity I, an alignment angle θ, and a pulse width $\tau_{\rm FWHM}$ is equal to the final population difference calculated at an intensity $I' = I\cos^2\theta$ and an alignment angle $\theta' = 0$ to a good approximation, that is, $\Delta p_{BvXv'}(I, \theta, \tau_{\rm FWHM}) \approx \Delta p_{BvXv'}(I\cos^2\theta, 0, \tau_{\rm FWHM})$. Therefore when investigating the dependence of $\Delta p_{BvXv'}$ on I, θ, and $\tau_{\rm FWHM}$, it is sufficient to calculate $\Delta p_{BvXv'}$ as a function of I and $\tau_{\rm FWHM}$ at $\theta = 0$. After obtaining $\Delta p_{BvXv'}(I, \theta = 0, \tau_{\rm FWHM})$, the θ dependence of $\Delta p_{BvXv'}$ can be calculated according to $\Delta p_{BvXv'}(I, \theta, \tau_{\rm FWHM}) \approx \Delta p_{BvXv'}(I\cos^2\theta, 0, \tau_{\rm FWHM})$. In order to confirm that the approximation of $\Delta p_{{\rm B}vXv'}(I, \theta, \tau_{\rm FWHM}) \approx \Delta p_{BvXv'}(I\cos^2\theta, 0, \tau_{\rm FWHM})$ holds, we have performed a numerical simulation at $\tau_{\rm FWHM} = 50$ fs, $\theta = 0°$, and $I = \cos^2 65° \times 8 \times 10^{13}$ W/cm^2 $= 1.4 \times 10^{13}$ W/cm^2 and compared the results with the simulation conducted at $\tau_{\rm FWHM} = 50$ fs, $\theta = 65°$, and $I = 8 \times 10^{13}$ W/cm^2 shown in Fig. 4(b). The final population differences between the $B\,^2\Sigma_u^+(1)$ state and the $X\,^2\Sigma_g^+(2)$ state are $\Delta p_{B1X2}(8 \times 10^{13}\ {\rm W/cm^2}, 65°, 50\ {\rm fs}) = 8.3\%$ and $\Delta p_{B1X2}(1.4 \times 10^{13}\ {\rm W/cm^2}, 0°, 50\ {\rm fs}) = 9.3\%$, and those for the $B\,^2\Sigma_u^+(0)$ state and the $X\,^2\Sigma_g^+(1)$ state are $\Delta p_{B0X1}(8 \times 10^{13}\ {\rm W/cm^2}, 65°, 50\ {\rm fs}) = 5.6\%$ and $\Delta p_{B0X1}(1.4 \times 10^{13}\ {\rm W/cm^2}, 0°, 50\ {\rm fs}) = 7.3\%$, both of which show that $\Delta p_{BvXv'}(I, \theta, \tau_{\rm FWHM}) \approx \Delta p_{BvXv'}(I\cos^2\theta, 0, \tau_{\rm FWHM})$ is a good approximation.

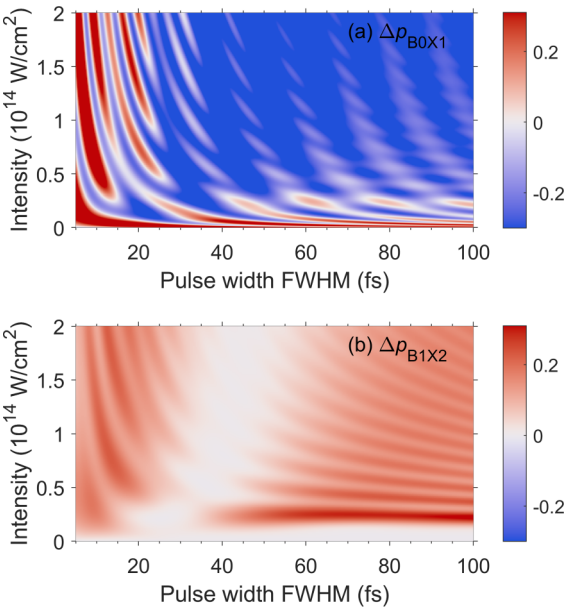

FIG. 5. Final difference of the populations in (a) the $B\,^2\Sigma_u{}^+(0)$ state and the $X\,^2\Sigma_g{}^+(1)$ state, $\Delta p_{B0X1} = p_{B0}(t_{\rm final}) - p_{X1}(t_{\rm final})$, and (b) the $B\,^2\Sigma_u{}^+(1)$ state and the $X\,^2\Sigma_g{}^+(2)$ state, $\Delta p_{B1X2} = p_{B1}(t_{\rm final}) - p_{X2}(t_{\rm final})$, as a function of the pulse width and the laser intensity. The alignment angle is set to be $\theta = 0^\circ$ in both (a) and (b). The numerical values of the population differences are shown by the color bars. The same color range is used in both (a) and (b). The population inversion is achieved in the red regions ($\Delta p_{B_v X_{v'}} > 0$), and no population inversion is achieved in the blue regions.

In Fig. 5(a) we show the final population difference $\Delta p_{B0X1} = p_{B0}(t_{\rm final}) - p_{X1}(t_{\rm final})$ between the $B\,^2\Sigma_u{}^+(0)$ state and the $X\,^2\Sigma_g{}^+(1)$ state as a function of the pulse width $\tau_{\rm FWHM}$ and the laser intensity I. In Fig. 5(b) we show the final population difference $\Delta p_{B1X2} = p_{B1}(t_{\rm final}) - p_{X2}(t_{\rm final})$ between the $B\,^2\Sigma_u{}^+(1)$ state and the $X\,^2\Sigma_g{}^+(2)$ state. We can see in Fig. 5(a) that $\Delta p_{B0X1} < 0$ in the large parameter ranges of $I > 3 \times 10^{13}$ W/cm^2 and $\tau_{\rm FWHM} > 25$ fs, and that population inversion ($\Delta p_{B0X1} > 0$) can be achieved only when $\tau_{\rm FWHM} < 25$ fs or when $I < 2 \times 10^{13}$ W/cm^2. On the other hand, the final population difference Δp_{B1X2} between the $B\,^2\Sigma_u{}^+(1)$ state and the $X\,^2\Sigma_g{}^+(2)$ state shown in Fig. 5(b) is always positive except for very small laser intensities $I < 5 \times 10^{12}$ W/cm^2. We conclude that the population inversion between the $B\,^2\Sigma_u{}^+(1)$ state and the $X\,^2\Sigma_g{}^+(2)$ state can be achieved in the broad ranges in laser intensity and the laser pulse duration, that is, 5×10^{12} W/cm^2 $< I < 2 \times 10^{14}$ W/cm^2 and 5 fs $< \tau_{\rm FWHM} < 100$ fs.

We also investigate the influence of variations in the ionization time t_0 on the final populations. We have performed simulations for the case of $\tau_{\rm FWHM} = 50$ fs and $I = 8 \times 10^{13}$ W/cm^2 where the simulation is started at different timings of $t = t_0$. We denote the final population in state $\alpha(v)$ obtained at an ionization time t_0 and an alignment angle θ as $p^{\rm final}_{\alpha v}(t_0, \theta)$. The θ-dependent final population averaged over t_0 is defined as

$$p^{\rm av}_{\alpha v}(\theta) = N \int_{-\infty}^{\infty} dt_0 \Gamma_{\rm MOSFA}[f(t_0), \theta] p^{\rm final}_{\alpha v}(t_0, \theta), \qquad (2)$$

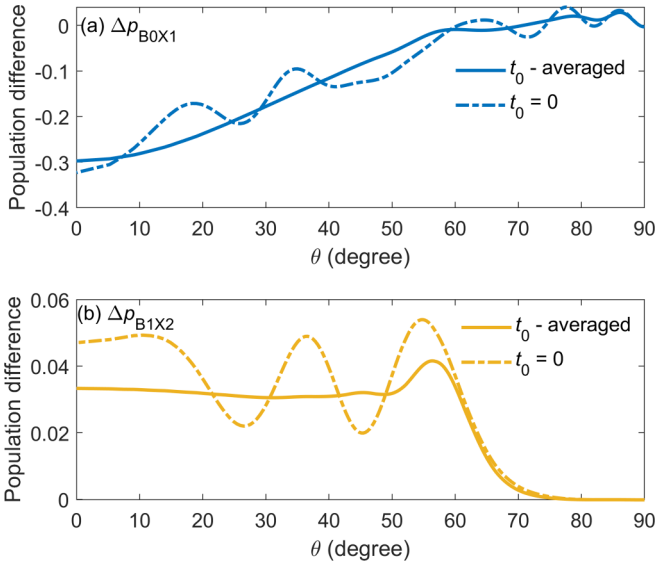

FIG. 6. (a) The final population difference between the $B\,^2\Sigma_u{}^+(0)$ state and the $X\,^2\Sigma_u{}^+(1)$ state and (b) that between the $B\,^2\Sigma_u{}^+(1)$ state and the $X\,^2\Sigma_u{}^+(2)$ state. Two approximations are compared: (i) the population calculated by averaging over the ionization time t_0 in the range of $-98 < t_0 < 98$ fs as defined in Eq. (2) (labeled "t_0-averaged") and (ii) the population obtained by including the contribution only from $t_0 = 0$ (labeled "$t_0 = 0$"). The laser field intensity is 8×10^{13} W/cm^2, and the pulse duration is 50 fs.

where N is a normalization constant defined so that $\sum_{\alpha,v} \int_0^\pi d\theta \sin\theta p^{\rm av}_{\alpha v}(\theta) = 1$, $\Gamma_{\rm MOSFA}[f(t_0), \theta]$ is the length gauge MO-SFA ionization rate [44], and $f(t_0) = F_0 e^{-t_0^2/\sigma^2}$ is the envelope of the laser pulse. In the numerical evaluation of Eq. (2), we approximate the integral over t_0 by a discrete sum over $t_{0n} = n\pi/2\omega$ with integer n in the range $-300 \leqslant n \leqslant 300$, corresponding to the time range of $-98 < t_0 < 98$ fs, and neglect the $A\,^2\Pi_u - X\,^2\Sigma_g{}^+$ coupling in the calculation of $p^{\rm final}_{\alpha v}(t_0, \theta)$.

In Fig. 6 we show the population differences $\Delta p^{\rm av}_{B0X1}(\theta) = p^{\rm av}_{B0}(\theta) - p^{\rm av}_{X1}(\theta)$ and $\Delta p^{\rm av}_{B1X2}(\theta) = p^{\rm av}_{B1}(\theta) - p^{\rm av}_{X2}(\theta)$ and compare the two cases of (i) the population differences calculated by the averaging over t_0 in the range of $-98 < t_0 < 98$ fs as defined in Eq. (2), and (ii) the population differences achieved only by the ionization at $t_0 = 0$. As can be seen in Fig. 6, even though the final population difference for the case of $t_0 = 0$ oscillates as a function of the alignment angle and this oscillation is averaged out by the averaging over t_0, the overall behavior of the θ dependence for the case of $t_0 = 0$ is consistent with that obtained by the averaging over t_0.

If we consider an isotropic rotational distribution of the molecular axis at the delay time of 420 fs, the total final population difference $\Delta p^{\rm tot}_{\alpha v \alpha' v'}$ can be obtained by integrating $\Delta p^{\rm av}_{\alpha v \alpha' v'}$ over θ:

$$\Delta p^{\rm tot}_{\alpha v \alpha' v'} = \int_0^\pi d\theta \sin\theta \Delta p^{\rm av}_{\alpha v \alpha' v'}(\theta). \qquad (3)$$

We obtain $\Delta p^{\rm tot}_{B0X1} = -11\%$ and $\Delta p^{\rm tot}_{B1X2} = 4.0\%$ for the population differences averaged over t_0, which means that at $I = 8 \times 10^{13}$ W/cm^2, population inversion between the $B\,^2\Sigma_u{}^+(1)$ state and the $X\,^2\Sigma_g{}^+(2)$ state is also achieved when

we consider the contributions from all alignment angles θ, which is consistent with the experimental observation of the 423.6-nm lasing line. On the other hand, $\Delta p^{\rm tot}_{B0X1}$ is negative, suggesting that population inversion between the $B\,^2\Sigma_u^+(0)$ state and the $X\,^2\Sigma_g^+(1)$ state is not achieved at the intensity of $I = 8 \times 10^{13}\,\mathrm{W/cm^2}$. Because the simulation results shown in Fig. 5(a) suggest that population inversion between the $B\,^2\Sigma_u^+(0)$ state and the $X\,^2\Sigma_g^+(1)$ state is achieved for intensities smaller than $2 \times 10^{13}\,\mathrm{W/cm^2}$, one possibility is that the lasing at 427.8 nm is emitted from the peripheral parts of the filament column where the intensity is smaller than the clamping intensity estimated to be in the range of 8×10^{13}–$16 \times 10^{13}\,\mathrm{W/cm^2}$.

IV. SUMMARY

We have investigated both experimentally and theoretically the $B\,^2\Sigma_u^+ - X\,^2\Sigma_g^+$ (0, 1) and (1, 2) lasing actions of N_2^+ at 427.8 nm and 423.6 induced by a 400-nm laser field. By examining both the self-induced and externally seeded forward emission spectra, we have unambiguously identified that the population-inverted N_2^+ can be created by the intense 400-nm laser pulse. The numerical simulations have revealed that the population in N_2^+ can be efficiently transferred between the $X\,^2\Sigma_g^+$ state and the $B\,^2\Sigma_u^+$ state by the Rabi oscillation combined with the simultaneous Raman-type transitions, leading to the population-inverted N_2^+. This mechanism of the lasing of N_2^+ at 400 nm, that is, the lasing achieved by the vibrationally mediated Rabi oscillation, is the lasing action characteristic of molecular species in which molecular vibration plays a crucial role in a different manner from the lasing induced by an intense 800-nm laser field where the $A\,^2\Pi_u$ state plays an important role [23]. We have also demonstrated that in the 400-nm laser pumping scheme, the population inversion occurs between the $B\,^2\Sigma_u^+(1)$ state and the $X\,^2\Sigma_g^+(2)$ state in the broad ranges of the laser field intensity ($5 \times 10^{12}\,\mathrm{W/cm^2} < I < 2 \times 10^{14}\,\mathrm{W/cm^2}$) and the pulse duration ($5\,\mathrm{fs} < \tau_{\rm FWHM} < 100\,\mathrm{fs}$), that is, the population inversion is not sensitive to the variations in the laser parameters, which exhibits marked differences from the population inversion between the $B\,^2\Sigma_u^+(0)$ state and the $X\,^2\Sigma_g^+(1)$ state, which occurs only in the specific ranges of the laser parameters. The theoretical simulations have shown that in order for the population inversion between the $B\,^2\Sigma_u^+(0)$ state and the $X\,^2\Sigma_g^+(1)$ state to be realized, at least one of the following conditions need to be satisfied: (i) the laser intensity should be smaller than $2 \times 10^{13}\,\mathrm{W/cm^2}$, and (ii) the laser pulse width has to be smaller than 25 fs.

ACKNOWLEDGMENTS

This work is supported in part by the National Natural Science Foundation of China (Contracts No. 61625501, No. 62027822, and No. 11904121), the State Key Laboratory of High Field Laser Physics (open fund), the Education Department of Jilin Province (JJKH20200938KJ), and JSPS KAKENHI Grants No. JP15H05696 and No. JP20H00371.

[1] H. L. Xu, Y. Cheng, S. L. Chin, and H. B. Sun, Laser Photon. Rev. **9**, 275 (2015).
[2] Q. Luo, W. Liu, and S. L. Chin, Appl. Phys. B **76**, 337 (2003).
[3] A. Dogariu, J. B. Michael, M. O. Scully, and R. B. Miles, Science **331**, 442 (2011).
[4] H. Zang, H. Li, W. Zhang, Y. Fu, S. Chen, H. Xu, and R. Li, Light Sci. Appl. **10**, 49 (2021).
[5] A. Laurain, M. Scheller, and P. Polynkin, Phys. Rev. Lett. **113**, 253901 (2014).
[6] D. Kartashov, S. Ališauskas, G. Andriukaitis, A. Pugžlys, M. Shneider, A. Zheltikov, S. L. Chin, and A. Baltuška, Phys. Rev. A **86**, 033831 (2012).
[7] S. Mitryukovskiy, Y. Liu, P. Ding, A. Houard, and A. Mysyrowicz, Opt. Express **22**, 12750 (2014).
[8] J. Yao, B. Zeng, H. Xu, G. Li, W. Chu, J. Ni, H. Zhang, S. L. Chin, Y. Cheng, and Z. Xu, Phys. Rev. A **84**, 051802(R) (2011).
[9] T. J. Wang, J. Ju, J. F. Daigle, S. Yuan, R. Li, and S. L. Chin, Laser Phys. Lett. **10**, 125401 (2013).
[10] Y. Liu, Y. Brelet, G. Point, A. Houard, and A. Mysyrowicz, Opt. Express **21**, 22791 (2013).
[11] J. Yao, W. Chu, Z. Liu, J. Chen, B. Xu, and Y. Cheng, Appl. Phys. B **124**, 73 (2018).
[12] H. Li, D. Yao, S. Wang, Y. Fu, and H. Xu, Chin. Phys. B **28**, 114204 (2019).
[13] J. Ni, W. Chu, C. Jing, H. Zhang, B. Zeng, J. Yao, G. Li, H. Xie, C. Zhang, H. Xu, S. L. Chin, Y. Cheng, and Z. Xu, Opt. Express **21**, 8746 (2013).
[14] H. Xu, E. Lötstedt, A. Iwasaki, and K. Yamanouchi, Nat. Commun. **6**, 8347 (2015).
[15] Y. Liu, P. Ding, G. Lambert, A. Houard, V. Tikhonchuk, and A. Mysyrowicz, Phys. Rev. Lett. **115**, 133203 (2015).
[16] J. Yao, S. Jiang, W. Chu, B. Zeng, C. Wu, R. Lu, Z. Li, H. Xie, G. Li, C. Yu, Z. Wang, H. Jiang, Q. Gong, and Y. Cheng, Phys. Rev. Lett. **116**, 143007 (2016).
[17] Y. Zhang, E. Lötstedt, and K. Yamanouchi, J. Phys. B **52**, 055401 (2019).
[18] Y. Zhang, E. Lötstedt, and K. Yamanouchi, Phys. Rev. A **101**, 053412 (2020).
[19] A. Azarm, P. Corkum, and P. Polynkin, Phys. Rev. A **96**, 051401(R) (2017).
[20] D. Kartashov, S. Haessler, S. Ališauskas, G. Andriukaitis, A. Pugžlys, A. Baltuška, J. Möhring, D. Starukhin, M. Motzkus, A. M. Zheltikov, M. Richter, F. Morales, O. Smirnova, M. Y. Ivanov, and M. Spanner, in *Conference on High Intensity Lasers and High Field Phenomena* (Optical Society of America, Washington, DC, 2014), Paper No. HTh4B.5.
[21] A. Mysyrowicz, R. Danylo, A. Houard, V. Tikhonchuk, X. Zhang, Z. Fan, Q. Liang, S. Zhuang, L. Yuan, and Y. Liu, APL Photonics **4**, 110807 (2019).
[22] M. Richter, M. Lytova, F. Morales, S. Haessler, O. Smirnova, M. Spanner, and M. Ivanov, Optica **7**, 586 (2020).
[23] T. Ando, E. Lötstedt, A. Iwasaki, H. Li, Y. Fu, S. Wang, H. Xu, and K. Yamanouchi, Phys. Rev. Lett. **123**, 203201 (2019).
[24] H. Xu, E. Lötstedt, T. Ando, A. Iwasaki, and K. Yamanouchi, Phys. Rev. A **96**, 041401(R) (2017).

[25] H. Li, M. Hou, H. Zang, Y. Fu, E. Lötstedt, T. Ando, A. Iwasaki, K. Yamanouchi, and H. Xu, Phys. Rev. Lett. **122**, 013202 (2019).
[26] A. Zhang, Q. Liang, M. Lei, L. Yuan, Y. Liu, Z. Fan, X. Zhang, S. Zhuang, C. Wu, Q. Gong, and H. Jiang, Opt. Express **27**, 12638 (2019).
[27] A. Zhang, M. Lei, J. Gao, C. Wu, Q. Gong, and H. Jiang, Opt. Express **27**, 14922 (2019).
[28] H. Xie, Q. Zhang, G. Li, X. Wang, L. Wang, Z. Chen, H. Lei, and Z. Zhao, Phys. Rev. A **100**, 053419 (2019).
[29] Y. Fu, E. Lötstedt, H. Li, S. Wang, D. Yao, T. Ando, A. Iwasaki, F. H. M. Faisal, K. Yamanouchi, and H. Xu, Phys. Rev. Res. **2**, 012007(R) (2020).
[30] H. Li, E. Lötstedt, H. Li, Y. Zhou, N. Dong, L. Deng, P. Lu, T. Ando, A. Iwasaki, Y. Fu, S. Wang, J. Wu, K. Yamanouchi, and H. Xu, Phys. Rev. Lett. **125**, 053201 (2020).
[31] G. Li, H. Xie, Q. Zhang, H. Lei, X. Zhou, X. Wang, Z. Chen, and Z. Zhao, Opt. Lett. **45**, 5616 (2020).
[32] T. Wang, J. Daigle, J. Ju, S. Yuan, R. Li, and S. L. Chin, Phys. Rev. A **88**, 053429 (2013).
[33] J. Daigle, A. Jaron-Becker, S. Hosseini, T. Wang, Y. Kamali, G. Roy, A. Becker, and S. L. Chin, Phys. Rev. A **82**, 023405 (2010).
[34] C. Jing, H. Zhang, W. Chu, H. Xie, J. Ni, B. Zeng, G. Li, J. Yao, H. Xu, Y. Cheng, and Z. Xu, Opt. Express **22**, 3151 (2014).
[35] F. Théberge, W. Liu, P. Simard, A. Becker, and S. Chin, Phys. Rev. E **74**, 036406 (2006).
[36] R. R. Laher and F. R. Gilmore, J. Phys. Chem. Ref. Data **20**, 685 (1991).
[37] W. Liu and S. L. Chin, Opt. Express **13**, 5750 (2005).
[38] X.-L. Liu, W. Cheng, M. Petrarca, and P. Polynkin, Opt. Lett. **41**, 4751 (2016).
[39] H. Li, W. Chu, H. Zang, H. Xu, Y. Cheng, and S. L. Chin, Opt. Express **24**, 3424 (2016).
[40] K. P. Huber, G. H. Herzberg, J. W. Gallagher, and R. D. Johnson III, Constants of diatomic molecules, in *NIST Chemistry WebBook*, NIST Standard Reference Database Number 69, edited by P. J. Linstrom and W. G. Mallard (National Institute of Standards and Technology, Gaithersburg, MD, 2021).
[41] S. R. Langhoff, C. W. Bauschlicher, and H. Partridge, J. Chem. Phys. **87**, 4716 (1987).
[42] S. R. Langhoff and C. W. Bauschlicher, Jr., J. Chem. Phys. **88**, 329 (1988).
[43] J. Tross, X. Ren, V. Makhija, S. Mondal, V. Kumarappan, and C. Trallero-Herrero, Phys. Rev. A **95**, 033419 (2017).
[44] T. K. Kjeldsen and L. B. Madsen, J. Phys. B: At. Mol. Opt. Phys. **37**, 2033 (2004).